Studies of Millimeter-wave Phenomenology for Helicopter Brownout Mitigation

Christopher A. Schuetz[b], E. Lee Stein Jr. [a], Jesse Samluk[a], Daniel MacKrides[a], John P. Wilson[a], Richard D. Martin[b], Thomas E. Dillon[b], and Dennis W. Prather[a]*

[a] Dept of Electrical and Computer Engineering, University of Delaware, 140 Evans's Hall, Newark, DE 19716 USA

[b] Phase Sensitive Innovations, Inc., 51 East Main St, Suite 201, Newark, DE 19711 USA

ABSTRACT

The unique ability of the millimeter-wave portion of the spectrum to penetrate typical visual obscurants has resulted in a wide range of possible applications for imagers in this spectrum. Of particular interest to the military community are imagers that can operate effectively in Degraded Visual Environments (DVE's) experienced by helicopter pilots when landing in dry, dusty environments, otherwise known as "brownout." One of the first steps to developing operational requirements for imagers in this spectrum is to develop a quantitative understanding of the phenomenology that governs imaging in these environments. While preliminary studies have been done in this area, quantitative, calibrated measurements of typical targets and degradation of target contrasts due to brownout conditions are not available. To this end, we will present results from calibrated, empirical measurements of typical targets of interest to helicopter pilots made in a representative desert environment. In addition, real-time measurements of target contrast reduction due to brownout conditions generated by helicopter downwash will be shown. These data were acquired using a W-band, dual-polarization radiometric scanner using optical-upconversion detectors.

Keywords: Millimeter-wave phenomenology, brownout, DVE- Degraded Visual Environment

1. INTRODUCTION

In recent years, millimeter-wave imaging has demonstrated many potential applications due to the unique capabilities of this portion of the spectrum to penetrate typical obscurants, while maintaining sufficient spatial resolution for many applications. One application that received significant interest in recent years is using millimeter-wave imagery to aid helicopter pilots landing in Degraded Visual Environments (DVE's). The most common DVE condition prevalent in today's theater of operations is that caused by blowing dust and sand, otherwise known as "brownout". Several studies in laboratory environments have indicated that attenuation due to suspended dust at millimeter-wave frequencies is low when compared to other bands [1,2]. However, to our knowledge, no field data has been taken on dust attenuation due to actual helicopter generated dust in a representative environment. Herein, we present some of the first ever measurements of passive millimeter-wave contrast reduction due to helicopter induced brownout. In addition to measurements of the atmospheric channel, we have also imaged a cross-section of typical landing-zone obstacles in a representative environment. Each image was taken on each of two linear polarization states with a temperature-calibrated radiometer. The data taken during this data collection compares favorably with previously reported results [3], albeit with higher contrasts perhaps due to the lower effective sky temperatures encountered in the Arizona desert, where this data was measured. Finally, we have used the captured phenomenology data to generate a scene simulation tool based on the open source ray-tracing software Blender, which will also be presented herein.

2. EQUIPMENT

For all of the data presented herein, the imager used was a dual-polarization scanning radiometer based on optical upconversion detection [4,5]. This imager uses a single-dish antenna with a 0.6 m primary aperture and an adjustable

Millimetre Wave and Terahertz Sensors and Technology II, Edited by Keith A. Krapels, Neil A. Salmon, Proc. of SPIE Vol 7485, 74850F, ©2009 SPIE CCC code: 0277-786X/09/$18 doi:10.1117/12.830480

http://dx.doi.org/10.1117/12.830480

secondary to focus energy from a single point in the scene into a scalar horn antenna. The antenna assembly is mounted on an az-el gimbal with a pointing accuracy of ~0.01°. To create an image, the antenna is raster scanned across the desired field of view with data gathered continuously as the imager is swept. Captured field-of-view, sweep time, and angular resolution are all adjustable in software. The Cassegrain antenna simultaneously collects both horizontal and vertical polarizations, which are separated after the scalar horn via an orthomode transducer and fed to two independent millimeter-wave radiometric detector assemblies with responsivity over the full W-band. A schematic diagram of the utilized detector assemblies is shown schematically in Figure 1.

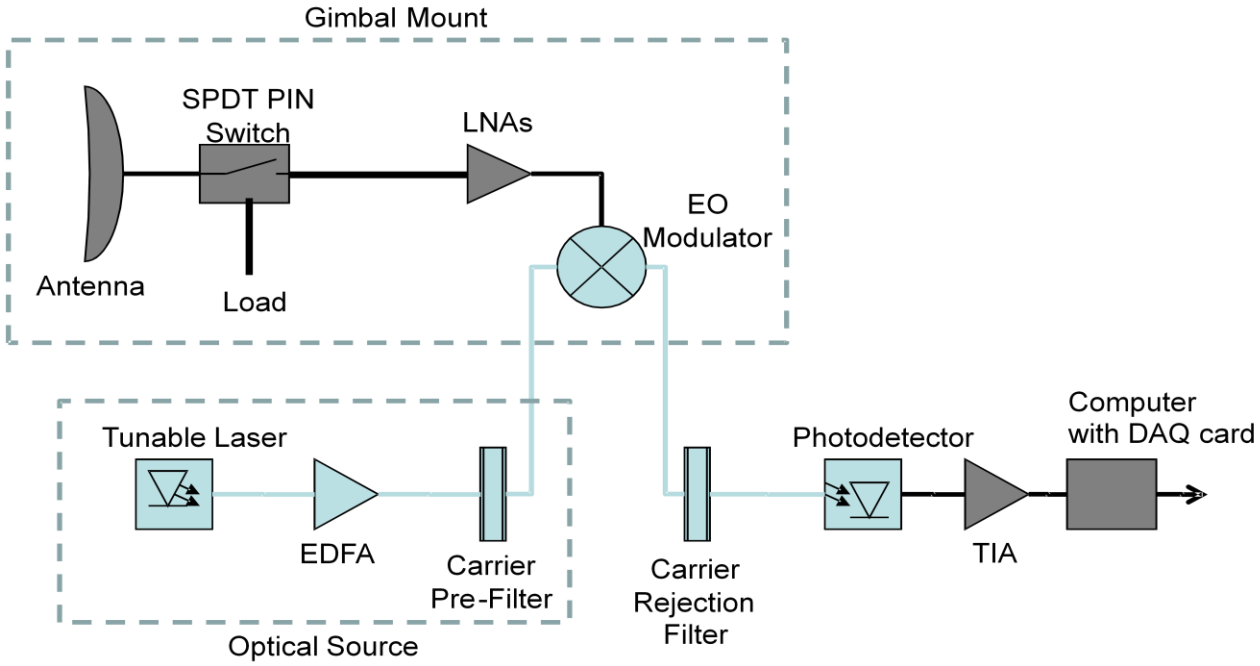

Figure 1. Schematic representation of a single channel of the detector assembly used in the radiometric imager for this testing.

The detector assembly consists of a front end PIN switch that is used to chop the signal between the scene and a known resistive load at a frequency of approximately 2 KHz in a process similar to Dicke switching. The output of the PIN switch is fed to a chain of two full W-band LNA's with a nominal gain of ~18dB each. The output of the LNA's is connected to a custom W-band optical modulator fabricated by PSI. The input of the optical modulator is fed by a filtered optical source that consists of a tunable laser, EDFA, and optical filtering. The upconverted output is fed to a second optical filter, which serves to reject the energy of the optical carrier. The filtered, upconverted energy is then detected using a PIN photodiode and amplified using a transimpedance amplifier. The output of the transimpedance amplifier is digitized on a computer DAQ card and the resulting chop signal is extracted using custom algorithms. This chop signal is representative of the scene temperature, and upon calibration with a pair of known temperature scenes, the absolute temperature of the scene can be derived. To create an image, the gimbal mounted antenna is raster scanned with synchronous collection of the radiometric temperature.

The overall result of the described hardware configuration is a scanning imager with an NETD of ~2K on each channel when using a 20 msec integration time. At this integration time, the imager is able to capture a 20°×30° field-of-view image with a 0.2° step size in ~10 minutes. The spatial resolution of the imager was confirmed to be near diffraction-limited with a spatial resolution of ~5 cm when the Cassegrain secondary was focused to the nominal imaging distance of 7 meters used for the majority of the images collected. For the flyover brownout testing, the secondary was set for optimal angular resolution in the far field, which was nominally 7 mrad, and the integration time was adjusted for each of the passes to trade temporal resolution for noise performance with an accordant square root scaling in the measured NETD.

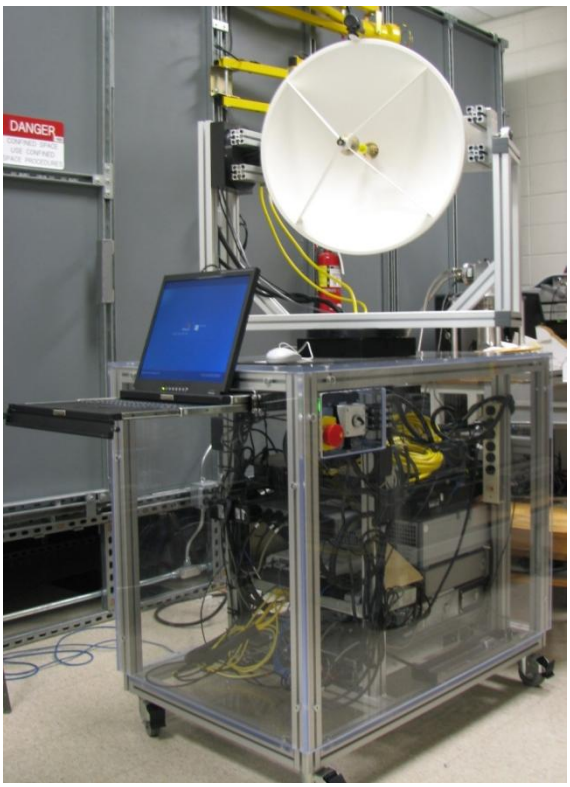

Figure 2. Picture of completed radiometric imager used in these data collections.

3. CALIBRATION

An important part of this data collection was to collect temperature calibrated imagery so that the absolute radiometric temperature difference of targets in the scene could be derived. Accurate temperature calibration in a field data collection often presents significant challenges due to the difficulties obtaining a pair of high-emissivity radiometric sources with a wide temperature differential that can cover the large effective apertures of the imaging antenna. Temperature targets with near ambient temperatures may be accomplished by using a piece of anechoic absorber material whose physical temperature is monitored by means of an embedded thermocouple. However, to obtain a radiometric temperature calibration at a minimum a second temperature calibration point is required, preferably with a large temperature difference. To accomplish this second data point, the dish was pointed towards zenith sky temperature and the detector was calibrated assuming a zenith sky temperature of 40 K. This zenith sky temperature was calculated using a Naval Research Laboratory internal model, based on Wentz statistical data, which uses local weather conditions to predict sky temperature and is in line with other published literature for the dry desert conditions experienced during the data collection. The model was run for a range of sky conditions and yielded a worst case deviation of 10K for the range of possible conditions experienced during the data collection. In addition, the model was compared against an azimuthal sweep of sky temperature measured using the radiometer calibrated to the assumed zenith sky temperature as shown in Figure 3. This sweep further validates the temperature calibration as the profile of temperature with zenith angle is dependent on atmospherically induced absorption. The slight deviation between modeled and measured data is believed to be due to the measured data actually collecting over a ~2.4º range of zenith angles as the secondary was kept set to a nominal 7-meter focus for the static imager testing and was not reset for collection of calibration data. The imager was calibrated against zenith sky temperature and temperature-monitored anechoic material prior to each data image acquisition to assure that drift in the sensor did not affect the temperature

calibration of the acquired images. In addition, at no time during the testing period were atmospheric conditions observed that could significantly change the zenith sky temperature that was used as a calibration point (e.g. no cloud cover).

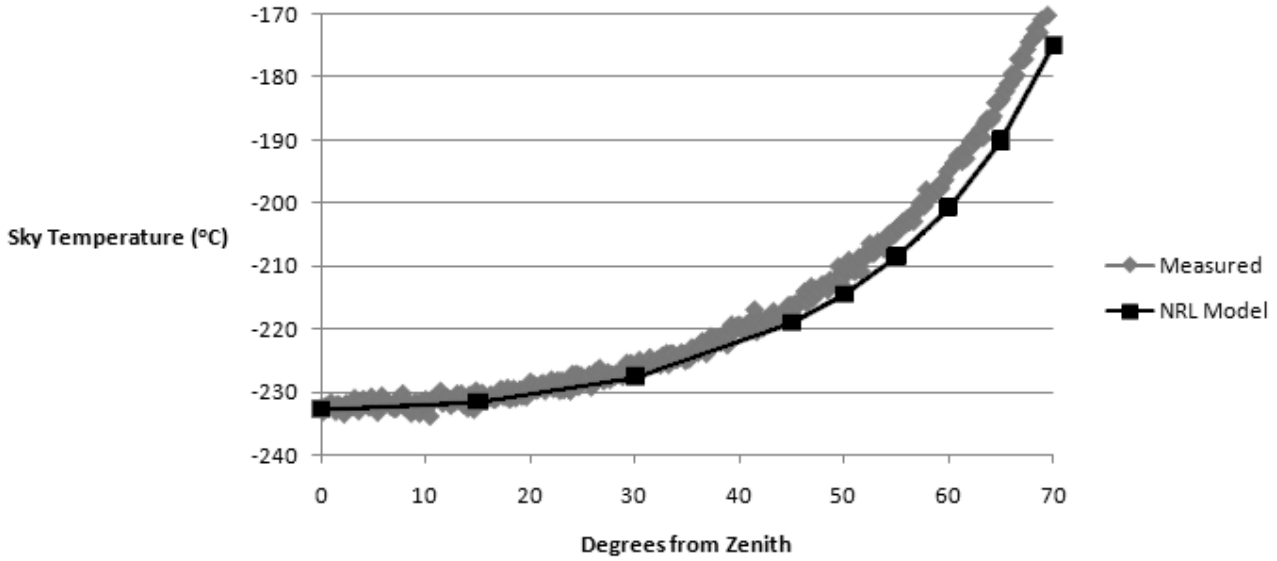

Figure 3. Plot of sky temperature as a function of angel from zenith as predicted by the NRL model described herein and as measured calibrated to a zenith sky temperature of 40K.

4. BROWNOUT TESTING

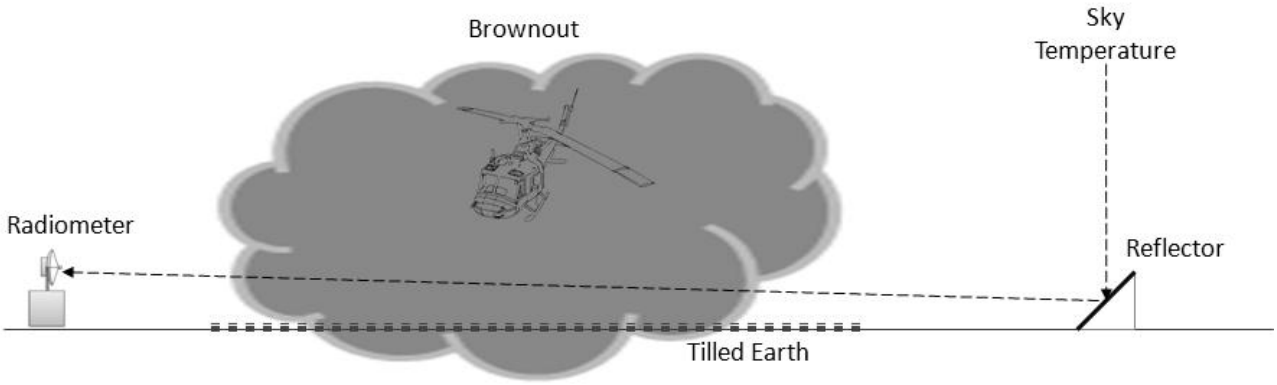

Figure 4. Pictorial representation of setup for testing of absorption/scattering due to helicopter-induced brownout.

To validate the use of millimeter-wave imaging for brownout mitigation, it is important to quantify the effects of dust on atmospheric propagation. As an initial test of these effects, we measured the radiometric obscuration of a high contrast target while the path was obscured by brownout generated by a helicopter flyover. For this test, the imager was configured to collect data from a single point and record the data as a function of time. The imager was then aligned to an 8' square reflector placed on the other side of a flyover lane at a distance of ~240' and angled so as to reflect zenith sky temperature as shown in Figure 4. Raw temperature data was then recorded for both polarization states as a function of time during five successive helicopter passes. Sample data sets are shown in Figure 5. The data set shows recorded temperature as a function of time. Prior to testing, the alignment of the radiometer to the reflector was chosen

to minimize the temperature readout. In this manner, any misalignment due to wind or other effects during data collection should present themselves as larger reductions in contrast than actually imposed.

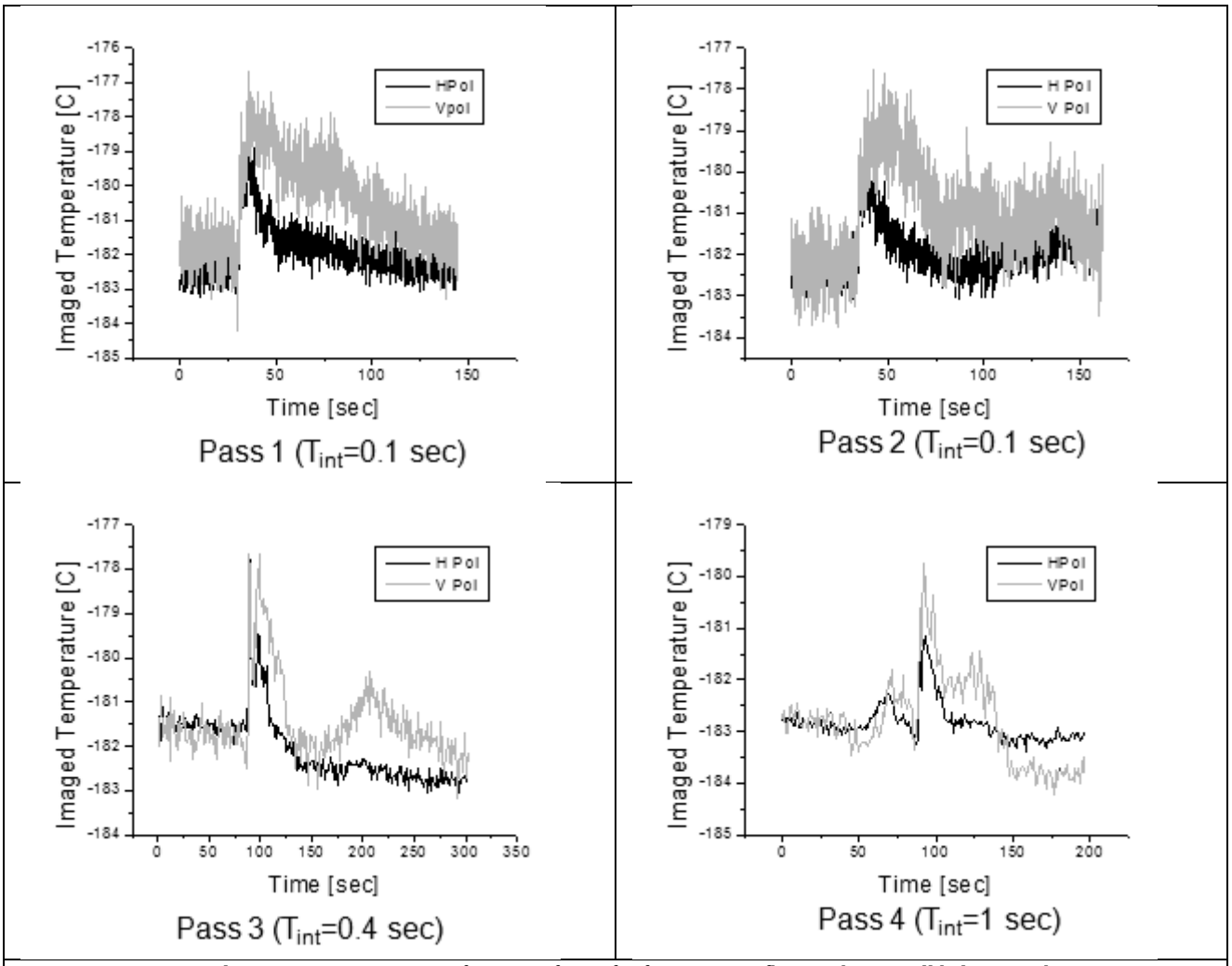

Figure 5. Radiometric temperature as a function of time for four separate flyovers by a small helicopter showing a worst case induced peak of 4ºC. Integration time of the detector was varied to trade temporal resolution for noise performance over the course of the four tests.

The fundamental mechanisms that reduce the measured reflector temperature could be absorption, scattering, or a combination of the both. If the reduction in temperature is assumed to be due to absorption, as obscurants pass between the reflector and the imager, the recorded temperature should warm towards the approximate ambient temperature at the time of test of 30°C. During the five passes tested during this data collection, the maximum increase in temperature recorded was 4°C out of a possible absorption-based increase of ~210°C as can be seen in Figure 5. Thus, the maximum observed contrast degradation was less than 2% even under the heaviest brownout conditions observed for this airframe. Assuming the reduction in image contrast is entirely due to absorption, this value would correspond to an average absorption over the 240' measurement path of 1.14 dB/km. However, it is important to note that the airframe used presented a moderately low level of disc loading for a military airframe and that larger airframes will present

significantly higher dust densities due to their higher disc loads. Further, testing of dust attenuation due to brownout induced by larger airframes will be acquired over the course of the next year.

5. STATIC IMAGERY

A second data point necessary in determining system requirements for brownout mitigation using passive millimeter-wave imagery is the temperature contrast of targets in this regime. To this end, calibrated radiometric imagery of several objects common to in-theater helicopter landing zones were taken. A cross-section of this imagery in shown in Figure 6 below.

Visible Image	Horizontal Polarization	Vertical Polarization
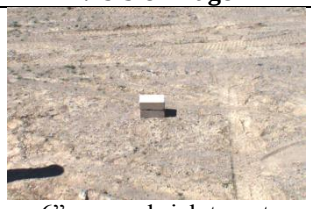 6" square brick target	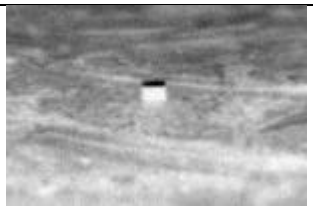	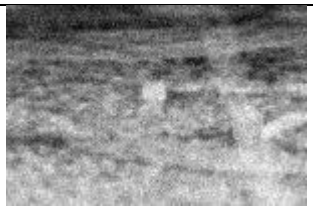
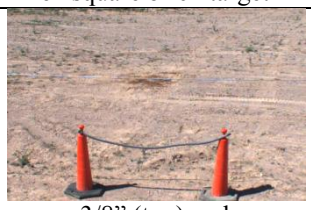 3/8" (top) and 1" (bottom) wire	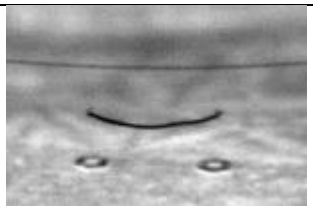	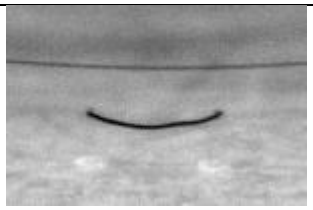
 2' Diameter Hole	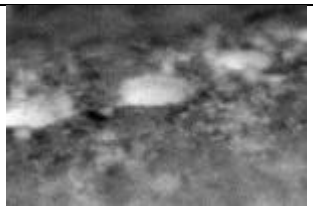	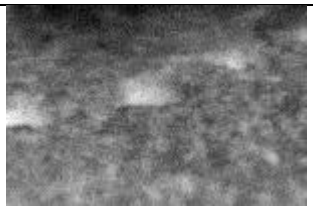
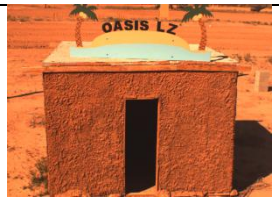 Adobe hut with person inside		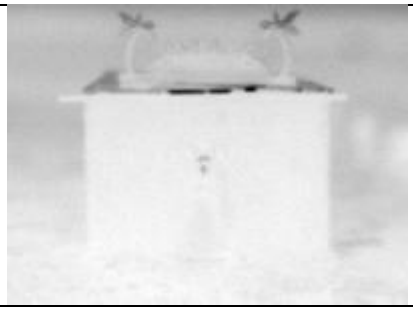

Helicopter

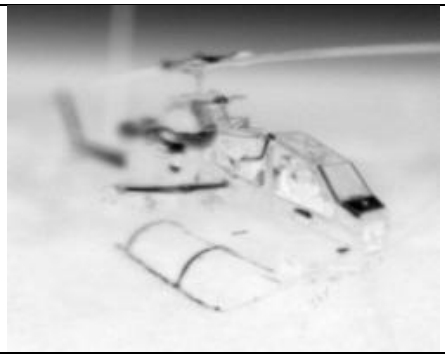

Figure 6. Cross section of static imagery collected. Imagery is normalized within each image to maximize presented contrast with white representing the radiometrically warmest part of the image.

All images during this data collection were acquired using the radiometric setup described above with a nominal distance to target of 7 meters. Since radiometric contrast is a function of incidence angle due to the strong gradation of sky temperature, the imager was lifted to a height of 3 meters above ground level to simulate an anticipated helicopter approach angle of ~25°. Imagery was taken for approximately 23 different landing zone obstacles. For several simple objects, the temperature contrast yielded by the object against a packed dirt background was analyzed quantitatively using a target contrast measurement routine developed by the Night Vision and Electronic Sensors Directorate for target contrast analysis of infrared imagery. This routine analyzes the root-sum-squared (RSS) temperature delta of a target by comparing the target (as delineated by a user-defined area in the image) with the background defined by an equivalent area outside the delineated target area. Table 1 shows a listing of measured RSS temperature differences for several of the targets tested during this data collection

Table 1. Measured radiometric temperature contrasts of common landing zone obstacles against packed dirt.

Object Description	Visible image in Figure 7	H-Polarization RSS Target Contrast	V-Polarization RSS Target Contrast
14 cm Width Wooden Post	a	25 K	10 K
0.6m Diameter Hole in Soil	b	16 K	6 K
0.6m Basaltic Rock	c	15 K	6 K
Cinder Block	d	17 K	3 K
Stack of Adobe Bricks-Front Aspect	e	20 K	5 K
Stack of Adobe Bricks-Top Aspect	e	28 K	3 K

(a) (b) (c) (d) (e)

Figure 7. Visible imagery of targets contrasts presented in Table 1.

From these data, it is readily apparent that for this application, E-field polarized parallel to the horizon (H-polarization) presents far better temperature contrast that the orthogonal V-polarization. This effect is due primarily to the significantly higher reflection coefficient of packed dirt to the parallel polarization state, which provides lower background temperatures due to the effective cold sky temperatures.

6. CONCLUSIONS AND FURTHER WORK

Preliminary testing of phenomenology in unimproved landing zones similar to those in current military theater of operations has demonstrated favorable conditions for the use of passive-millimeter imaging as a brownout mitigation tool. Direct testing of brownout conditions for a small military helicopter yielded only a 2% degradation in contrast even when visual operation was completely obscured. In addition, effective thermal contrasts on the order of 15 K or more were measured for most of the common landing zone obstacles measured when using a horizontally polarized radiometer. This relatively high temperature contrast lowers system constraints required to effectively perform obstacle detection for landing in brownout conditions. Although preliminary indications are favorable, further testing is required to validate the findings of this study. First, the effects of higher dust densities due to larger airframes will be evaluated in the next few months. In addition, the relative contributions of scattering and absorption to contrast degradation in brownout at these wavelengths must be further evaluated to determine the final effect on acquired image quality in such degraded visual conditions.

7. ACKNOWLEDGMENTS

We would like to thank the Office of Naval Research - Command, Control Communications, Intelligence, Surveillance, and Reconnaissance (C4ISR) Division, the Naval Research Laboratory – Remote Sensing Division, and NAVAIR PMA-261- H53Heavy Lift Helicopters Division for generously sponsoring and supporting various aspects of this work. In addition, we would like to specifically thank Walt Harrington at the Air Force Research Laboratory (AFRL-RYZC) for providing access to test facilities and air support for the presented data and Night Vision and Electronic Sensors Directorate for providing analysis tools for quantifying target contrasts.

8. BIBLIOGRAPHY

[1] Wikner, D., “Millimeter-wave propagation through a controlled dust environment”, Proceedings of SPIE, v 6548, (2007).

[2] Nüßler, D., Essen, H., Von Wah, N., Zimmermann, R., Rötze, S., Willms, I., “Millimeter wave propagation through dust”, Proceedings of SPIE, v 7108, (2008).

[3] Wikner, D. A., “Passive millimeter-wave imagery of helicopter obstacles in a sand environment”, Proceedings of SPIE, v 6211, (2006).

[4] Samluk, J. P., Schuetz, C. A., Stein, E. L., Robbins, A., Mackrides, D. G., Martin, R. D., Caihua, C., Prather, D. W., “Far field millimeter-wave imaging via optical upconversion”, Proceedings of SPIE, v 6948, (2008).

[5] Schuetz, C. A., Murakowski, J.; Schneider, G. J.; Prather, D. W. , “Radiometric millimeter-wave detection via optical upconversion and carrier suppression”, IEEE Transactions on Microwave Theory and Techniques, v 53, n 5, p 1732-1738, May (2005).